Journal of Fluorescence, Vol. 16, No. 3, May 2006 (© 2006)
DOI: 10.1007/s10895-005-0045-9

Photoluminescence and Optical Absorption of $Cs_2NaScF_6:Cr^{3+}$

L. P. Sosman,[1] R. J. M. da Fonseca,[1] A. Dias Tavares Jr.,[1,4] M. K. K. Nakaema,[2] and H. N. Bordallo[3]

Received June 20, 2005; accepted December 5, 2005
Published online: June 7, 2006

The main objective of this paper is the characterization of the spectroscopic properties of new materials that are prospective laser media. This approach allows for the comparison of the properties of the Cr^{3+} in different environments. Here, we have studied the photoluminescence and optical absorption of $Cs_2NaScF_6:Cr^{3+}$ single crystals. On the basis of near-infrared luminescence measurements at 2, 77, and 300 K the observed lines originated from the Cr^{3+}-centres were associated with the ${}^4T_2({}^4F) \rightarrow 4A_2({}^4F)$ transition and the lifetimes were obtained. In spite of the quenching observed as a function of temperature at least 10% of the 2 K emission intensity for Cs_2NaScF_6 doped with 1% of Cr^{3+} remains at room temperature. Besides, the 2 K emission broad band could be well described in terms of normal modes of the octahedral complex $[CrF_6]^{3-}$, and the Racah and crystal-field parameters calculated.

KEY WORDS: insulators; crystal and ligand fields; chromium; time-resolved optical spectroscopy.

INTRODUCTION

There is renewed interest in solid-state optical materials that emit in the visible and near infrared spectral region [1–7]. In particular, materials doped with transitions metal ions have been intensively studied due to their inherent tunability and possible applications as signal transmission, display devices, information storage [8,9]. Several Cr^{3+}-doped materials have been studied, mainly due to the strong visible absorption and emission bands observed when the Cr^{3+} ion is incorporated into octahedrally coordinated sites. The unfilled 3d electronics shell of the Cr^{3+} ion has a number of low-lying energy levels, among which optical transitions can occur generating luminescent emission. As in the transition metal ions the 3d electrons are outside of the ion core, they interact strongly with the electric field of the nearby ions, so their optical properties are directly affected by static and dynamic properties of their environment. Furthermore, both sharp transitions and broad emission bands can occur at low temperature in the optical 3d ions spectra. While the sharp transitions occur between levels that do not depend on the crystal field intensity, the broad bands are attributed to transitions between electronic states derived from the crystal field orbitals that present different dependencies on crystal field strength. Indeed, the separation between the energy levels is very sensitive to the *Dq* parameter value and their transitions are characterized by larger values of the Huang–Rhys parameter [10]. In addition, these broad bands have a great interest in tunable laser materials at 300 K. However, as the electron–phonon coupling can enhance nonradiative decay processes, leading to a decrease in the luminescence quantum yield, and minimizing non-radiative decays, it is useful to choose materials with small phonon energies [11].

Several studies on fluorides compounds doped with transition metal ions have been reported in the literature

[1] Instituto de Física, Universidade do Estado do Rio de Janeiro, 20559-900, RJ Brazil.
[2] IFGW-DFESCM, Universidade Estadual de Campinas, 13083-970, SP, Brazil.
[3] Hahn-Mettner Institut-Berlin, D-14109, Germany
[4] To whom correspondence should be addressed. E-mail: tavares@uerj.br.

[12–21], and its is now well established that they present long upper-state lifetimes, and are, consequently, potential materials to be used as efficient amplifying media. Moreover, the observation of a broad red absorption bands allows direct diode pumping. Therefore, our interest in the optical characterization of the fluoride Cs_2NaScF_6:Cr^{3+} through luminescence and absorption techniques in order to verify its possible application as a tunable laser material.

The system studied here, Cs_2NaScF_6, belongs to the group A_2BMX_6, where A and B are monovalent alkali cations, M is a trivalent cation and X is a monovalent anion (see Fig. 1). The analogous systems Cs_2NaAlF_6 and Cs_2NaGaF_6 show hexagonal structure with $R3\bar{m}$ symmetry, with the trivalent cations ordered and octahedrally surrounded by F anions [22–24]. On the basis of our optical results we can assume that the Cr^{3+} ions are also octahedrally coordinated and replace the Sc^{3+} ions. Using phase-resolved emission measurements, we were unable to find evidence for more than one lifetime, and so concluded that the Cr^{3+} ions are occupying only one kind of site. In addition, from the emission spectra measured at 2, 77, and 300 K and from absorption spectrum measured at 300 K, we could assign the energy levels of the chromium ion in the host material. From the 300 K absorption spectrum we calculated the crystal-field parameter Dq and Racah parameter B. The value of $Dq/B \sim 2$ indicates that the energy levels of the $^4T_2(^4F)$ and $^2E(^2G)$ are very close to each other.

EXPERIMENTAL DETAILS

The 2 K photoluminescence experiments were performed using a He-cryostat and those at 77 K with an immersion cryostat. The exciting source was a cw 514.5 nm line from a Coherent Radiation Ar-ion laser model 52. The excitation intensity was switched on and off at a reference frequency using a SR 540 variable speed chopper. The sample emission was analyzed with an Spex model 1870 spectrometer. A liquid N_2 cooled RCA S1 photomultiplier coupled to a SR 530 lock-in detected the optical signals at a reference frequency. The absorption measurements were achieved with a CAM SPEC M 330 spectrometer. Both emission and absorption measurements were corrected for the response of the monochromator and detection system.

The Cs_2NaScF_6:Cr^{3+} samples are single crystals grown by the hydrothermal method with 1.0% of Cr^{3+} ion as impurity. The fluorides were synthesized by the direct temperature-gradient method as a result of the reaction of aqueous solutions of CsF (30–35 mol%) and NaF. The

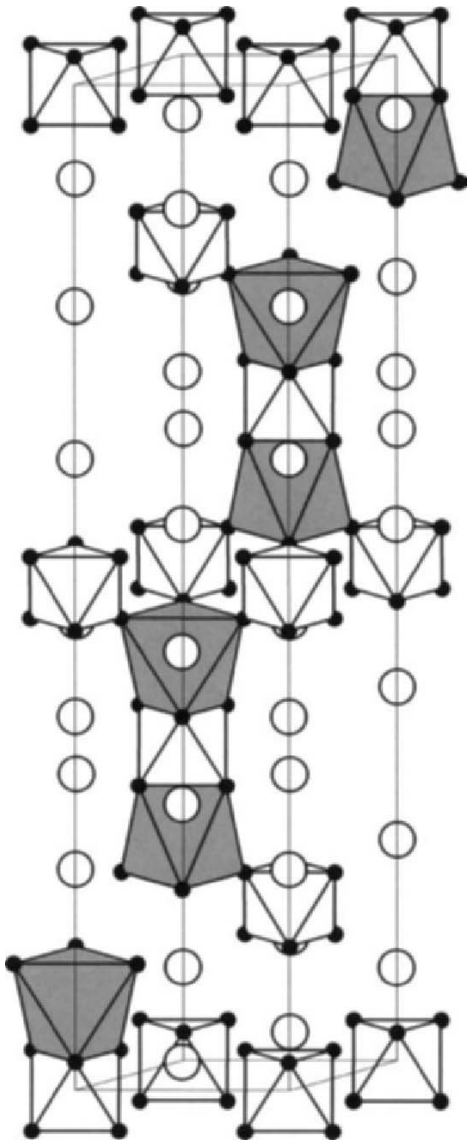

Fig. 1. Polyhedral representation of the Cs_2NaScF_6:Cr^{3+} structure. The white and gray polyhedra represent ScF_6 and NaF_6, respectively, while the white and gray atoms correspond to Cs and F.

mole ratio CsF/NaF changed from 4.8 to 5.2 with appropriate oxide mixtures of Sc_2O_3 and Cr_2O_3 (99.995% pure) at a temperature about 750 K, a temperature gradient of about 2 K/cm and pressures of 100–150 Mpa [25]. The substitution of oxygen by fluorine in oxides is easy due to the similar size of the O^{2-} and F^- anions. The referred structures for which the substitution can occur are rutiles, perovskites, and garnets [26]. For hydrothermal experiments, autoclaves with copper liners having a volume of about 40 cm^3 were utilized. Under these conditions, spontaneously nucleated crystals up to 0.5 cm^3 in

size were grown in the upper region of the autoclave. The obtained crystal phase homogeneity and the possible distortions of crystal lattice were tested by the X-ray powder diffraction method. Considering that the most important factors for substitution are the ionic radius ($r_{Sc}{}^{3+} = 0.73$Å and $r_{Cr}{}^{3+} = 0.615$ Å) and the valence that is the same for the Ga and Cr ions, we can argue that the Cr^{3+} ions enter in host replacing the Sc^{3+} ions.

RESULTS AND DISCUSSION

Figure 2 presents the Cs_2NaScF_6 photoluminescence spectra of 1.0% Cr^{3+} at 300 K (a), 77 K (b), and 2 K (c). The emission bands are identified as the phonon assisted $^4T_2(^4F) \rightarrow {}^4A_2(^4F)$ transition of the forbidden *d–d* crystal field levels of Cr^{3+} ions in octahedral sites [27]. As the $^4T_2$ state has a $t_2{}^2e$ configuration and the $^4A_2$ state has $t_2{}^3$ configuration, the $^4T_2$–$^4A_2$ transition is broad. The relaxation process at 300 K originates an emission band at

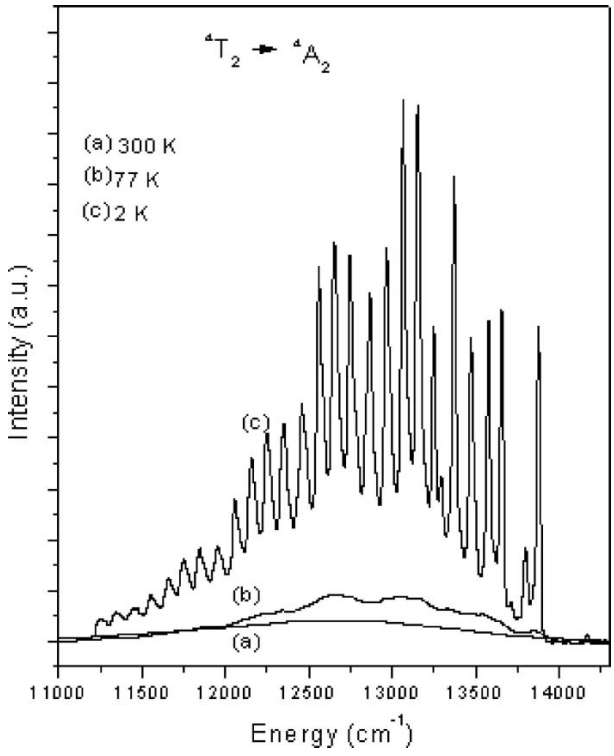

Fig. 2. The photoluminescence spectra of Cs_2NaScF_6 doped with 1.0 at.% Cr^{3+} at (a) 300 K, (b) 77 K, and (c) 2 K. At 300 K the luminescence lifetime measured through the phase-sensitive detection was $\tau_{300\ K} = 117\ \mu$s, while at 77 K, $\tau_{77\ K} \sim 4\ \tau_{300\ K}$. This observation is an indication that the Cr^{3+} ions occupy undistinguished octahedral sites in the host structure.

12626 cm^{-1} observed in Fig. 2(a). In this temperature, the luminescence lifetime measured through the phase-sensitive detection was $\tau_{300\ K} = 117\ \mu$s. As it was not possible to verify two different occupation sites for the Cr^{3+} ions at 300 K, we assume that this decay time as an average value. The 77 K emission spectrum, Fig. 2(b), exhibits two intense peaks at 13055 and 12658 cm^{-1} and a number of weaker emissions. For this emission the measured lifetime with phase-shift method was $\tau_{77\ K} = 414\ \mu$s, which differs only by a factor 4 of $\tau_{300\ K}$, indicating that the emission at 77 K can be associated to the $^4T_2\ (^4F) \rightarrow {}^4A_2\ (^4F)$ transition as well. Some samples with Cr^{3+} in intermediate crystalline field, can present emissions at low temperature from the level ^2E [28–30]. However, these forbidden spin transitions present, generally, a lifetime of the order of a few milliseconds. As the observed transitions at room temperature and at 77 K in Cs_2NaScF_6 have the same order of lifetime, this can indicate that they originate from the same level, $^4T_2\ (^4F)$. Considering the similar energy position, the band shape, as well as the value of the measured lifetimes, we can argue that the 300 K spectrum has the same origin of the low temperature spectrum, the $^4T_2$ level. The observed quenching of the emission (Fig. 2) as a function of temperature for the low-field sites will be discussed later.

The complete luminescence spectrum at 2 K for Cs_2NaScF_6:1.0 %Cr^{3+} is shown in Fig. 3. The low temperature $^4T_2\ (^4F) \rightarrow {}^4A_2\ (^4F)$ emission exhibits a very rich fine structure, superposed to a broad vibronic band that extends from 13875 cm^{-1} to 11248 cm^{-1}. From this spectrum the Huang–Rhys factor S was calculated, with $e^{-S} = I_{ZPL}/I$ [1], where I and I_{ZPL} are the integrated intensity in the broadband and zero-phonon line, respectively. For $Cs_2NaScF_6:Cr^{3+}$ this parameter was found to be 3.6. This value is compatible with the $^4T_2\ (^4F) \rightarrow {}^4A_2\ (^4F)$ assignment, for which Huang–Rhys factor has to be bigger than 1, and in agreement with the S values obtained for $K_2NaScF_6:Cr^{3+}$ and $K_2NaGaF_6:Cr^{3+}$, 3.95 and 3.98, respectively [17,28].

The analysis of the luminescence spectrum in terms of the normal modes of vibration of $[CrF_6]^{3-}$ octahedral complex, was made in analogy to $K_2NaScF_6:Cr^{3+}$ [2,17–19] that presents similar luminescence spectra. In order to verify if the lines observed in $Cs_2NaScF_6:Cr^{3+}$ originate from different sites, as in the similar compounds $Cs_2NaAlF_6:Cr^{3+}$ [23,29] and $Cs_2NaGaF_6:Cr^{3+}$ [24,30], we used a lock-in amplifier to select an appropriated phase, so that the line at 13875 cm^{-1} would be eliminated. As after this procedure, no lines remained in the spectrum, so we can suppose that all lines present close lifetimes, pointing out that the Cr^{3+} ions occupy undistinguished octahedral sites in the host structure. Besides,

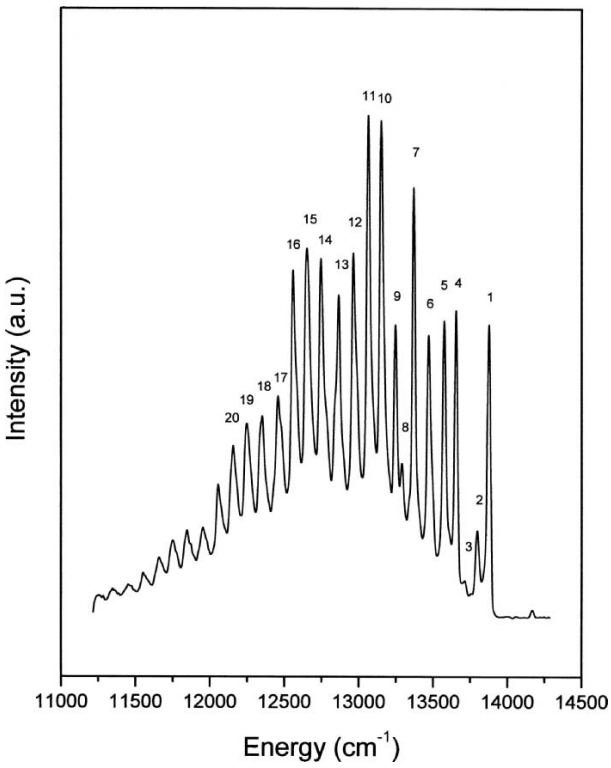

Fig. 3. The complete photoluminescence spectrum of Cs_2NaScF_6 doped with 1.0 at.% Cr^{3+} at 2 K. The zero-phonon, located at 13875 cm^{-1}, is indexed as line 1.

the luminescence lifetime measured for this transition is $\tau_{2\,K} = 443\ \mu s$, which is close to those obtained for similar systems [17–19,29, 30], where radiative recombination was not observed, showing that the luminescence data for Cs2NaScF6:Cr^{3+} originates from isolated impurity centers. In addition, the 300 K quantum efficiency (Φ) could be roughly estimated. Considering that $\Phi = \tau_{300\,K}/\tau_{2\,K}$ [1,31], and assuming that the temperature quenching is only due to nonradiative decays, one gets a Cr^{3+} emission quantum efficiency of about 0.3 at 300 K.

Now, we turn to the interpretation of the vibrational spectrum. In Cs_2NaScF_6:Cr^{3+} the dopant ion wave functions overlap with those of the six F^- nearly surrounding neighbors that is, in a simple form, represented by the combination of the Cr^{3+} plus the F^- contributions and forming the molecular orbital for the $[CrF_6]^{3-}$ octahedral complex. The Cr^{3+} form a 3d (t_{2g}, e_g), 4s (a_{1g}), 4p (t_{1u}) orbital, while the F^- group a $2p_\sigma$ (a_{1g}, $t_{1u,}$, e_g), $2p_\pi$ (t_{1u}, $t_{2g,}$, t_{2u}, t_{1g})., consequently the normal vibrations modes of $[CrF_6]^{3-}$ octahedral complex are given by $\Gamma^{vib} = a_{1g} + e_g + 2t_{1u} + t_{2g} + t_{2u}$ [32].

In Fig. 3, we can clearly observe the zero-phonon line located at 13875 cm^{-1}, line 1, and vibrational lines associated with the $^4T_2$ (^4F)→$^4A_2$ (^4F) transition, where the signal phase was adjusted to obtain the maximum intensity for line 1. In order to analyze the relative intensities (I_n/I_1) we have to consider the following. As the energy states of the Cr^{3+} ions have the same parity,

1. if the Cr^{3+} ion is in a site of inversion of symmetry, the allowed electronic transitions are of magnetic dipole, and therefore they have weak intensity. Thus, the magnetic dipole zero-phonon transition is ascribed with line at 13875 cm^{-1} (line 1);
2. on the other hand, if the Cr^{3+} ion is in a site without inversion of symmetry, the allowed electronic transitions are of electronic dipole, consequently with stronger intensity.

We can observe that all vibrational lines in 2 K spectrum are strong. Since the dopant ion is smaller than the Sc^{3+} ion, some strain is induced around Cr^{3+} ion and its ligand. This fact reduces the site symmetry and the 2 K emission spectrum is dominated by electric dipole vibronic band [33]. Consequently, the most intense sidebands at 13151 cm^{-1} (line 10) and at 13067 cm^{-1} (line 11) are associated with transitions produced by an odd-parity internal vibration of the complex $[CrF_6]^{3-}$, namely the t_{2u} (π) mode. Besides, the four strong vibronic peaks situated at 13651 (line 4), 13573 (line 5), 13470 (line 6) and 13369 cm^{-1} (line 7) can be, respectively, assigned as $t_{2u}(\pi)$, $t_{1u}(\pi)$, $e_g(\sigma)$ and $a_{1g}(\sigma)$ modes. Moreover, the σ orbitals are symmetric with respect to a rotation around the bond direction, while the π orbitals do not present this characteristic. So, the energy position of the $t_{1u}(\pi)$ mode (line 5) is expected to lie higher than that of the $t_{1u}(\sigma)$ mode (line 8). Furthermore, the relatively high intensity of the even modes, $e_g(\sigma)$ and a_{1g}, reflects the vicinity of the $^4T_2$ and the ^2E states [10], the reduction of the ion site symmetry and the possibility that Cr^{3+} ion can be displaced from the center of the octahedron [10,34]. Indeed, the observation of the electric dipole allowed $e_g(\sigma)$ progressions on the odd vibronic origins (line 9) gives further evidence to this assumption. As for $e_g(\sigma)$, the position of the mode $a_{1g}(\sigma)$ is also confirmed by the combination with some other lines with odd origin (lines 10 and 11). The apparent absence of the $t_{2g}(\pi)$ mode occurs because the relative intensities of vibrational lines related to this transition are very small and beyond the sensibility of the detection system [2,35]. The vibronic modes frequencies for Cs_2NaScF_6:Cr^{3+}, based on the electronic transition at 13875 cm^{-1}, are arranged in decreasing order and summarized in Table I. In this table, only intense lines in the higher energy positions at 2 K in the emission spectrum are identified. It is interesting to point out the energy intervals for phonon modes in different fluorides hosts, as summarized (in cm^{-1}) in reference [36]: a_{1g} (555–575), e_g (470–495), t_{1u} (560–590), t_{1u} (305–335) and

Table I. Experimental Positions and Assignment of the Labeled Peaks in the Emission Spectrum at 2 K for $Cs_2NaScF_6:Cr^{3+}$, Shown in Fig. 3

Line	Energy (cm^{-1})	Vibrational energy (cm^{-1})	Assignment
1	13 875	0	Zero-phonon line
2	13 797	78	lattice phonon modes
3	13 713	162	lattice phonon modes
4	13 651	224	t_{2u} (π)
5	13 573	302	t_{1u} (π)
6	13 470	405	e_g (σ)
7	13 369	506	a_{1g} (σ)
8	13 291	584	t_{1u} (σ)
9	13 249	626	t_{2u} (π) + e_g (σ)
10	13 151	724	t_{2u} (π) + a_{1g} (σ)
11	13 067	808	t_{2u} (π) + a_{1g} (σ) + 78
12	12 964	911	e_g (σ) + a_{1g} (σ)
13	12 866	1009	2 a_{1g} (σ)
14	12 746	1129	a_{1g} (σ) + t_{2u} (π) + e_g (σ)
15	12 652	1223	t_{2u} (π) + 2 a_{1g} (σ)
16	12 560	1315	t_{1u} (π)
17	12 458	1417	2 a_{1g} (σ) + e_g (σ)
18	12 351	1524	3a_{1g} (σ)
19	12 244	1631	2 a_{1g} (σ) + t_{2u} (π) + e_g (σ)
20	12 156	1719	2 a_{1g} (σ) + t_{1u} (π) + e_g (σ)

Note. The energies of vibrational modes are relative to that zero-phonon line.

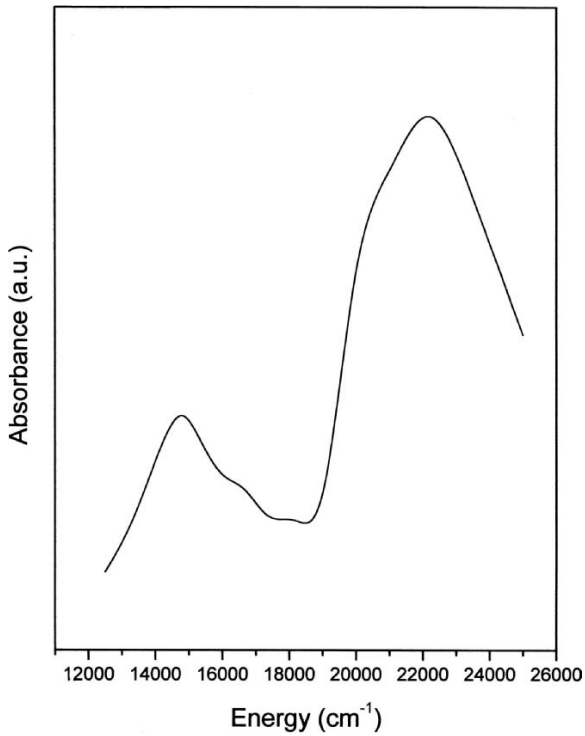

Fig. 4. Absorbance of Cs_2NaScF_6 doped with 1.0 at.% Cr^{3+} at 300 K. The band identified as $^4A_2$ (^4F)→$^4T_1$ (^4F) has its barycenter at 22050 cm^{-1}, and the band identified as $^4A_2$ (^4F)→$^4T_2$ (^4F) at 15000 cm^{-1}.

t_{2u} (160–220). In this paper, authors state that as e_g and a_{1g} modes undergo a decrease in their energies when the Cr^{3+}–F^- distance increases. At the same, time the energies of t_{1u} and t_{2u} are little affected by host distances changes. Accordingly this statement, the phonon modes in $Cs_2NaScF_6:Cr^{3+}$ are a indication of ion site distortion, which destroys the inversion site symmetry and can be associated with strong lines in 2 K spectrum.

The absorption spectrum of Cs_2NaScF_6:1% Cr^{3+} at 300 K is shown in Fig. 4. The band identified as $^4A_2$ (^4F)→$^4T_1$ (^4F) has its barycenter at 22050 cm^{-1}, while the lower energy band, identified as the $^4A_2$ (^4F)→$^4T_2$ (^4F) electronic transition of the Cr^{3+} center, at 15000 cm^{-1}. The comparison between the energy position of the $^4T_2$ (^4F)–$^4A_2$ (^4F) absorption and emission bands leads to a Stokes shift of 2374 cm^{-1}, a reasonable value for fluoride hosts [37]. From the $^4A_2$→$^4T_2$ (^4F) transition and the Tanabe–Sugano matrices for Cr^{3+} ($3d^3$) in octahedral environment [34], we can extract the cubic field splitting parameter 10Dq, and from the position of the $^4A_2$→T_1(^4F) transition we can estimate the Racah parameter B. For the free ions the Racah parameter is associated with Coulomb repulsion of electrons, while for crystals, it is influenced by the ligand anions and the metal cations, giving insight to the bond covalency. From well-known procedures [34], we obtain for Cs_2NaScF_6:1% Cr^{3+} a crystal field strength Dq equal to 1500 cm^{-1} and a Racah parameter B of 754 cm^{-1}. The Dq/B value, ~2, confirms, as mentioned above, that the $^4T_2$ and ^2E states are very close in energy, leading to intense e_g and a_{1g} modes [10].

Keeping in mind that we used an Argon laser with 8 W and a crystal size of 3 mm, giving an intensity of 280 kW/m^2, in the region of the laser spot, the real crystal temperature can be higher than 300 K. In spite of this fact a comparison of the integrated areas between the "room temperature" and the 2 K data was made and indicates that at least 10% of the 2 K-emission intensity for $Cs_2NaScF_6:Cr^{3+}$ remains at room temperature. The temperature dependence of the emission spectrum of Cr^{3+} has been systematically investigated [36,37], it can be ascribed to nonradiative relaxation mechanisms. Furthermore, due to the low concentration of the sample the energy transfer between the Cr^{3+} ions can be neglected.

CONCLUSIONS

In this paper, Cs_2NaScF_6 doped with 1.0 at.% of Cr^{3+} has been investigated by photoluminescence and optical absorption spectroscopy. The photoluminescence

spectra show broad vibronic bands between 11000 and 15000 cm^{-1}. The bands observed at 300, 77, and 2 K and the calculated crystal field parameter *Dq* lead us to conclude that the Cr^{3+} ions are octahedrally coordinated to the F^- ions in the host lattice. However, differently from $Cs_2NaAlF_6:Cr^{3+}$ and $Cs_2NaGaF_6:Cr^{3+}$ [23,24], only one luminescence lifetime was detected, indicating that as in $K_2NaScF_6:Cr^{3+}$ [2,17,19] the Cr^{3+} ion occupy only one type of octahedral site. Moreover, as the absorption signal of the $^4T_1$ (^4F) level is higher than that of the $^4T_2$ (^4F) level, and that a considerable number of Cr^{3+} ions decay radiationless from $^4T_1$ to $^4T_2$, favoring the emission $^4T_2 \rightarrow {}^4A_2$, the assignment of the emission bands as the $^4T_2$ (^4F)$\rightarrow {}^4A_2$ (^4F) transition is further supported. In addition, the vibrational spectrum was analyzed in terms of normal modes of the octahedral complex $[CrF_6]^{3-}$, leading to the conclusion that the $^4T_2$ (^4F) excited state is displaced along the e_g and a_{1g} coordinates. This displacement is analogous to that observed earlier in other fluoride compounds doped with Cr^{3+} ions, and attributed to Cr^{3+} ions in sites octahedrally coordinated by anions [35–39].

It is important to remember that nowadays the most efficient solid state laser is the $Be_3Al_2(SiO_3)_6:Cr3^+$, emitting between 11905 and 13889 cm^{-1}, with intensity peak at 13020 cm^{-1} and efficiency of 64% [40, 41], followed by $LiCaAlF_6:Cr^{3+}$ laser, with emission also between 11905 and 13889 cm^{-1}, maximum intensity at 12820 cm^{-1} and efficiency of 54% [42]. Systems with longer emission are the $LiSrAlF_6:Cr^{3+}$, emitting between 9900 and 12820 cm^{-1} with maximum at 12121 cm^{-1} and efficiency of 36% [43, 44] and the $La_3Ga_5SiO_{14}:Cr^{3+}$, tunable between 9033 and 11600 cm^{-1} with peak at 10330 cm^{-1}, but with only 10% of efficiency [45, 46]. Considering that the quantum efficiency of $Cs_2NaScF_6:Cr^{3+}$ is about 30%, its emission shows a peak 12626 cm^{-1} and 10% of 2 K emission intensity remains at room temperature, it is worth to study the suitability of this new Cr^{3+} doped material for laser application.

Additional X-ray and neutron diffraction experiments are in progress in order to investigate the crystal structure of $Cs_2NaScF_6:Cr^{3+}$, and Raman measurements are planned to probe the site symmetry of the Cr^{3+} this material.

ACKNOWLEDGMENTS

The authors are grateful to N. M. Khaidukov from the Institute of General and Inorganic Chemistry, Moscow, Russia, for providing the single crystal materials, and to F. Iikawa (IFGW–UNICAMP) and A. S. Luna (IQ–UERJ) for their assistance with PL and absorption measurements. This work was supported by FAPERJ and FINEP.

REFERENCES

1. S. Kück (2001). *Appl. Phys. B* **72**, 515–562.
2. G. R. Wein, D. S. Hamilton, U. Sliwczuk, A. G. Rinzler, and R. H. Bartram (2001). *J. Phys. Condens. Matt.* **13**, 2363–2375.
3. O. S. Wenger and H. U. Güdel (2001). *J. Chem. Phys.* **114**, 5832–5841.
4. T. Ohtake, N. Sonoyama, and T. Sakata (2000). *Chem. Phys. Lett.* **318**, 517–521.
5. T. Miyata, T. Nakatani, and T. Minami (2000). *J. Lumin.* **87–89**, 1183–1185.
6. A. P. Vink and A. Meijerink (2000). *J. Lumin.* **87–89**, 601–604.
7. S. Kück, L. Fornasiero, E. Mix, and G. Huber (2000). *J. Lumin.* **87–89**, 1122–1125.
8. H. W. H. Lee, S. A. Payne, and L. L. Chase (1989). *Phys. Rev. B* **39**, 8907–8914.
9. U. Brauch and U. Durr (1984). *Opt. Commun.* **49**, 61–64.
10. P. Greenough and A. G. Paulusz (1979). *J. Chem. Phys.* **70**, 1967–1972.
11. K. K. Rebane (1970). *Impurity Spectra of Solids*, 1st edn., Plenum Press, New York.
12. R. J. M. da Fonseca, L. P. Sosman, A. Dias Tavares Jr., and H. N. Bordallo (2000). *J. Fluoresc.* **10**, 375–381.
13. J. Ferguson, H. J. Guggenheim, and D. L. Wood (1971). *J. Chem. Phys.* **54**, 504–507.
14. U. Sliwczuk, R. H. Bartram, D. R. Gabbe, and B. C. McCollums (1991). *J. Phys. Chem. Solids* **52**, 357–361.
15. D. R. Lee, T. P. J. Han, and B. Henderson (1994). *Appl. Phys. A* **59**, 365–372.
16. M. Mortier, Q. Wang, J. Y. Buzaré, M. Rousseau, and B. Piriou (1997). *Phys. Rev. B* **56**, 3022–3031.
17. L. J. Andrews, A. Lempicki, B. C. McCollum, C. J. Giunta, R. H. Bartram, and J. F. Dolan (1986). *Phys. Rev. B* **34**, 2735–2740.
18. P. T. Kenyon, L. Andrews, B. McCollum, and A. Lempicki (1982). *IEEE J. Quantum Electron.* **QE18**, 1189–1196.
19. L. J. Andrews, S. M. Hitelman, M. Kokta, and D. Gabbe (1986). *J. Chem. Phys.* **84**, 5229–5238.
20. J. F. Dolan, A. G. Rinzler, L. A. Kappers, and R. H. Bartram (1992). *J. Phys. Chem. Solids* **53**, 905–912.
21. S. M. Healy, C. J. Donnelly, T. J. Glynn, G. F. Imbusch, and G. P. Morgan (1990). *J. Lumin.* **46**, 1–7.
22. E. Fargin, B. Lestienne, and J. M. Dance (1990). *Solid State Commun.* **75**, 769–771.
23. H. N. Bordallo, R. W. Henning, L. P. Sosman, R. J. M. da Fonseca, A. Dias Tavares Jr., K. M. Hanif, and G. F. Strouse (2001). *J. Chem. Phys.* **115**, 4300–4305.
24. H. N. Bordallo, X. Wang, K. M. Hanif, G. F. Strouse, R. J. M. da Fonseca, L. P. Sosman, and A. Dias Tavares Jr., (2002). *J. Phys. Condens. Matt.* **14** 12383–12389.
25. P. A. Tanner, L. Yulong, N. M. Edelstein, K. M. Murdoch, and N. M. Khaidukov (1997). *J. Phys. Cond. Matt.* 7817–7836.
26. P. Hagenmuller (1985). *Inorganic Solid Fluorides* 1st edn, Academic Press, USA.
27. Y. Tanabe and S. Sugano (1954). *J. Phys. Soc. Japan* **9**, 753–779.
28. M. Yamaga, B. Henderson, and K. P. O'Donnell (1992). *Phys. Rev. B* **46**, 3273–3282.
29. L. P. Sosman, A. D. Tavares Jr., R. J. M. da Fonseca, T. Abritta, and N. M. Khaidukov (2000). *Solid State Commun.* **114**, 661–665.
30. R. J. M. da Fonseca, A. D. Tavares Jr., P. S. Silva, T. Abritta, and N. M. Khaidukov (1999). *Solid State Commun.* **110**, 519–524.
31. O. S. Wenger and H. U. Güdel (2001). *J. Chem. Phys.* **114**, 5832–5841.

32. B. Di Bartolo (1968). *Optical Interactions in Solids*, 1st edn., Wiley, New York.
33. C. M. de Lucas, F. Rodriguez, J. M. Dance, M. Moreno, and A. Tressaud (1991). *J. Luminescence* **48–49**, 553–557.
34. B. Henderson and G. F. Imbusch (1989). *Optical Spectroscopy of Inorganic Solids*, 1st edn., Clarendon: Oxford.
35. U. Sliwczuk, R. H. Bartram, D. R. Gabbe, and B. C. McCollum (1991). *J. Phys. Chem. Solids* **532**, 357–361.
36. M. O. Ramirez, D. Jaque, M. Montes, J. Garcia Solé, and L. E. Bausá (2004) *Appl. Phys. Lett.* **84**, 2787.
37. U. R. Rodríguez-Mendoza, A. Speghini, D. Jaque, M. Zambelli, and M. Bettinelli (2004). *J. Alloys Comp.* **380**, 163.
38. B. Villacampa, R. Cases, and R. Alcalá (1995). *J. Lumin.* **63**, 289–296.
39. S. A. Payne, L. L. Chase, and W. F. Krupke (1987). *J. Chem. Phys.* **86**, 3455–3461.
40. M. L. Shand and S. T. Lai (1984). *IEEE J. Quantum Electron.* **20**, 105.
41. S. T. Lai (1987). *J. Opt. Soc. Am. B*, 1286.
42. S. A. Payne, L. L. Chase, H. W. Newkirk, L. K. Smith, and W. F. Krupke (1988). *IEEE J. Quantum Electron.* **24**, 2243.
43. M. Stalder, B. H. T. Chai, and M. Bass (1991). *Appl. Phys. Lett.* **58**, 216.
44. S. A. Payne, L. L. Chase, L. K. Smith, W. L. Kway, and H. W. Newkirk (1989). *J. Appl. Phys.* **6**, 1051.
45. S. T. Lai, B. H. T. Chai, M. Long, and M. D. Shinn (1988). *IEEE J. Quantum Electron.* **24**, 1922.
46. A. A. Kaminskii, A. P. Shkadarevich, B. V. Mill, V. G. Kuptev, and A. A. Demidovich (1987). *Inorg. Mater.* **23**, 618.